Available online at www.sciencedirect.com
ScienceDirect
Journal of Magnetic Resonance 183 (2006) 193–202
JMR Journal of Magnetic Resonance
www.elsevier.com/locate/jmr

How accurately can the diffusion profiles indicate multiple fiber orientations? A study on general fiber crossings in diffusion MRI

Wang Zhan, Yihong Yang *

Neuroimaging Research Branch, Intramural Research Program, National Institute on Drug Abuse, National Institutes of Health, Baltimore, MD 21224, USA

Received 5 October 2005; revised 26 July 2006
Available online 11 September 2006

Abstract

The q-space imaging techniques and high angular resolution diffusion (HARD) imaging have shown promise to identify intravoxel multiple fibers. The measured orientation distribution function (ODF) and apparent diffusion coefficient (ADC) profiles can be used to identify the orientations of the actual intravoxel fibers. The present study aims to examine the accuracy of these profile-based orientation methods by comparing the angular deviations between the estimated local maxima of the profiles and the real fiber orientation for a fiber crossing simulated with various intersection angles under different *b* values in diffusion-weighted MRI experiments. Both noisy and noise-free environments were investigated. The diffusion spectrum imaging (DSI), q-ball imaging (QBI), and HARD techniques were used to generate ODF and ADC profiles. To provide a better comparison between ODF and ADC techniques, the phase-corrected angular deviations were also presented for the ADC method based on a circular spectrum mapping method. The results indicate that systematic angular deviations exist between the actual fiber orientations and the corresponding local maxima of either the ADC or ODF profiles. All methods are apt to underestimation of acute intersection and overestimation of obtuse intersection angle. For a typical slow-exchange fiber crossing, the ODF methods have a non-deviation zone around the 90° intersection. Before the phase-correction, the deviation of ADC profiles approaches a peak at the 90° intersection, while after the correction the ADC deviations are significantly reduced. When the *b* factor is larger than 1000 s/mm^2, the ODF methods have smaller angular deviations than the ADC methods for the intersections close to 90°. QBI method demonstrates a slight yet consistent advantage over the DSI method under the same conditions. In the noisy environment, the mean value of the deviation angles shows a high consistency with the corresponding deviation in the nose-free condition.
Published by Elsevier Inc.

Keywords: Diffusion tensor imaging; Fiber crossing; High angular resolution diffusion imaging; Q-space imaging; Diffusion spectrum imaging

1. Introduction

Diffusion tensor imaging (DTI) has been established as a powerful tool for non-invasive investigation of white matter structures and connectivities in vivo [1–3]. Fiber tracking techniques have also been developed to delineate neural pathways based on the assumption that the major eigenvector of the diffusion tensor should be oriented parallel with local white matter fibers [4–6]. However, the validity of the DTI-based tractography is confounded by the fact that the primary eigenvector of the diffusion tensor may be seriously biased from the actual fiber direction if multiple fiber compartments share a single voxel [7,8]. This inability of DTI is technically due to the fact that the tensor model is a 2nd order approximation of a possible complex diffusion pattern [9], and consequently can provide only one global maximal direction corresponding to the primary eigenvector. In recent years, more elaborate acquisition and analysis strategies, including q-space imaging and high angular resolution diffusion (HARD) imaging techniques have been developed to tackle this challenge [10–24].

Q-space imaging techniques identify multiple fibers components by calculating the probability distribution function (PDF) of the diffusion process in each voxel, based on the Fourier transform (FT) relationship between

* Corresponding author. Fax: +1 410 550 1441.
E-mail address: yihongyang@intra.nida.nih.gov (Y. Yang).

1090-7807/$ - see front matter Published by Elsevier Inc.
doi:10.1016/j.jmr.2006.08.005

the PDF of diffusion displacement and the diffusion-weighted signal attenuation in q-space [10–12]. Even under the practical setting of finite pulse width, there is growing evidence that the estimated PDF is still a reasonable description of local diffusion and microstructural organization in brain tissues [13]. Diffusion spectrum imaging (DSI) has been proposed to estimate the diffusion PDF from a large number of data acquisitions in 3D q-space [14]. A study to assess the accuracy of DSI was performed on phantoms and animal models in practical MRI settings [15]. In DSI, the multiple fiber orientations are usually represented by the PDF angular structure, i.e. the orientation distribution function (ODF) that can be obtained by a radial integral of the PDF [15]. A modified technique, named q-ball imaging (QBI), has been proposed to acquire data only on a spherical surface in the q-space and to estimate the ODF directly from these data [16,17]. For both DSI and QBI methods, it is generally assumed that the multiple local maxima of the ODF profile should represent the actual orientations of multiple intravoxel fibers [15–17].

High angular resolution diffusion (HARD) techniques have also been developed to characterize the apparent diffusion coefficient (ADC) profiles for the intravoxel fibers [18–24]. Alexander et al. [20] and Frank [21] proposed the idea of using spherical harmonic decomposition (SHD) to characterize the 3-D apparent diffusion coefficient (ADC) profile measured by HARD imaging. In general, the lower order (0th or 2nd) spherical harmonics represent the isotropic diffusion or single fiber diffusion patterns, while the higher orders (4th or higher) represent non-Gaussian patterns associated with intravoxel multiple fiber components. Zhan et al. proposed a "diffusion circular spectrum mapping" (DCSM) method that examines only the ADC distribution along the circle spanned by the major and medium eigenvectors, and applies a 1-D FT onto this circular ADC distribution [22,23]. Unlike the q-space techniques, the local maxima of ADC profiles generally cannot be used to directly represent the orientations for the intravoxel crossing fibers. However, the orientations of the fiber crossings may be identified by incorporating both amplitude and phase information of the decomposed harmonics of the ADC profile, as demonstrated in [23].

The ability to identify fiber-crossings in both q-space and HARD imaging techniques stem from a common characteristic of ODF and ADC profiles, i.e. both methods allow multiple local maxima to appear on the estimated profiles. The angular accuracy of the local maxima in the profiles with respect to the actual fiber orientations would be crucial for the fiber tracking techniques because of the accumulative manner of the angular deviations along the tracking trajectory [15–17,19]. In previous studies, a mismatch between the orientation of a fiber crossing and the local maxima of its ADC profile has been pointed out [20,23,24], and the change of ODF profile sharpness has been reported [16,17]. Recently, Ozarslan et al. proposed a method applying the SHD technique to the ODF profiles and examined the orientation deviations for a few multiple fiber cases [25]. However, a systematic investigation onto the angular deviations between the local maxima of the ODF/ADC profiles and the orientations of the real intravoxel fibers have not yet been performed. The explicit relationship between the angular deviation and various conditions of the fiber crossing, e.g. the intersection angle, b factor, and noise level, remains unclear. Moreover, no effort has been reported in comparing the accuracy of identifying multiple-fiber orientations among various q-space and HARD imaging techniques. Resolving these issues is necessary to allow these beyond-tensor diffusion MRI techniques to serve as reliable tools in delineating white matter structures and neuronal pathways.

In this paper, a simulation study is presented to address the questions described above. A "general fiber crossing" with various intersection angles (0°–180°) is used to simulate the diffusion-weighting MRI experiments with different b values (1000–10,000 s^2/mm). The effects of imaging noise are also investigated by simulating both noise-free and noisy environments with different noise levels. The HARD, DSI and QBI techniques are implemented to estimate the ADC and ODF profiles of the general fiber crossing with various parameters. The angular deviations of the local maxima of the diffusion profiles are measured by the angle between the directions of the estimated local maxima and the known corresponding fiber orientations. To ensure a better comparison between ADC and ODF methods, the DCSM phase technique in [23] is also implemented to provide the corrected deviation angles for the ADC profiles.

2. Method

2.1. ADC modeling

The effective ADC profile $D(\theta,\phi)$ $(0 \leqslant \theta \leqslant \pi, 0 < \theta \leqslant 2\pi)$ of an ideal cylindrical symmetric single fiber can be written [26] as

$$D(\theta,\phi) = \frac{\mathbf{V}^{\mathrm{T}}}{\|\mathbf{V}\|} \cdot \mathbf{A}^{\mathrm{T}} \cdot \begin{bmatrix} \lambda_1 & & \\ & \beta\lambda_1 & \\ & & \beta\lambda_1 \end{bmatrix} \cdot \mathbf{A} \cdot \frac{\mathbf{V}}{\|\mathbf{V}\|} \tag{1}$$

where $\mathbf{V}$ denotes the vector of diffusion encoding direction and λ_1 is the maximal ADC measured in the direction parallel to the fiber. The ratio $0 < \beta < 1$ reflects the degree of linear anisotropy. $\mathbf{A}$ is the rotation matrix determined by the fiber orientation whose spherical coordinates (θ,ϕ) $(0 \leqslant \theta \leqslant \pi, 0 < \theta \leqslant 2\pi)$ represent the polar and azimuthal angle, respectively, such that

$$\mathbf{A} = \begin{bmatrix} \sin\phi & -\cos\phi & 0 \\ \cos\phi\cos\theta & \sin\phi\cos\theta & -\sin\theta \\ \cos\phi\sin\theta & \sin\phi\sin\theta & \cos\theta \end{bmatrix} \tag{2}$$

Thus, in a simulated ideal diffusion-weighted MRI experiment, the signal attenuation profile of this single fiber is given by $E = S/S_0 = \exp\{-bD(\theta,\phi)\}$, where b is the b factor used in the diffusion MRI experiment, while S and S_0 are the measured signal identities with and without the diffusion-weighting, respectively.

Let $D_1(\theta_1,\phi_1)$ and $D_2(\theta_2,\phi_2)$ be the ADC profiles of two intravoxel fibers that satisfy the relationships described in Eqs. (1) and (2). Under the condition of slow water exchange between the two fiber compartments, the equivalent signal attenuation profile of the fiber crossing can be estimated [27] by

$$E = f\cdot\exp\{-bD_1(\theta_1,\phi_1)\} + (1-f)\exp\{-bD_2(\theta_2,\phi_2)\} \tag{3}$$

where f and $(1-f)$ are the signal fractions representing the ratio of the first and second fibers sharing the voxel, respectively. The present investigation will focus on the typical fiber crossing of equal-fraction ($f = 0.5$) and fast water exchange. By using the partial voxel signal modeling of Eq. (3), the effective ADC profile of the intravoxel fiber crossing can be estimated by $D_{\text{app}}(\theta,\phi) = -\log(E)/b$.

Diffusion circular spectrum mapping (DCSM) methods [22,23] are used to obtain a phase-corrected angular deviation results for the ADC profile. For an equal-fraction slow-exchange fiber crossing, the 4th order harmonic of the circular spectrum can be written [23] as

$$\left|D^4_{\text{CS}}\right| = \frac{b(\beta-1)^2\lambda_1^2}{16}\cos[4\cdot\Omega] + \frac{b(\beta-1)^2\lambda_1^2 + 8(\beta+1)\lambda_1}{16}$$
$$\text{and}\quad \text{ang}\left\{D^4_{\text{CS}}\right\} = 4\cdot\Omega \tag{4}$$

where $|D^4_{\text{CS}}|$ and $\text{ang}\{D^4_{\text{CS}}\}$ are the magnitude and phase of the 4th order circular harmonic, respectively, whereas Ω denotes the crossing intersection angle between the two fibers. The phase-correction procedure [23] is applied to the fiber crossing with 4th order circular harmonic magnitude higher than the thresholding, i.e. $|D^4_{\text{CS}}| \geqslant 0.5\cdot b(\beta+1)\lambda_1$, which is corresponding to the fiber crossing with the intersection angle between 45° and 135°.

2.2. Diffusion spectrum imaging

In the context of the Stejskal and Tanner experiment [28] with a narrow width (δ) and a high magnitude of the diffusion-weighting pulsed gradients ($\mathbf{g}$), the MR echo attenuation $E(\mathbf{q})$ is related to the probability distribution function $\text{PDF}(\mathbf{r})$ of the diffusion displacement by a Fourier transform pair, i.e. $\text{PDF}(\mathbf{r}) = \text{FT}^{-1}\{E(\mathbf{q})\}$ [12], where $\mathbf{q}$ is the diffusion wavevector ($\mathbf{q} = (2\pi)^{-1}\cdot\gamma\cdot\delta\cdot\mathbf{g}$) in the q-space and $\mathbf{r}$ is the radial vector in the imaging space. For spherical coordinates, denote $\mathbf{q} = (r,\theta,\phi)$ and $\mathbf{r} = (R,\Theta,\Phi)$, the Fourier relationship can be rewritten as

$$\begin{aligned}\text{PDF}(R,\Theta,\Phi) = \int_0^{\pi}\int_0^{2\pi}\int_0^{\infty} & E(r,\theta,\phi)\\ &\times\exp\{2\pi jRr[\cos\Theta\cos\theta\\ &+\sin\Theta\sin\theta\cos(\phi-\Phi)]\}r^2\\ &\times\sin\theta\,\mathrm{d}r\,\mathrm{d}\phi\,\mathrm{d}\theta\end{aligned} \tag{5}$$

In the applications for identifying multiple intravoxel fibers, we are usually only interested in the angular structure of the PDF, thus the orientation distribution function $\text{ODF}(\Theta,\Phi)$ is defined as the radial projection of $\text{PDF}(R,\Theta,\Phi)$, such that

$$\begin{aligned}\text{ODF}(\Theta,\Phi) &= \int_0^{\infty}\text{PDF}(R,\Theta,\Phi)\,\mathrm{d}R\\ &= \int_0^{\pi}\int_0^{2\pi}\int_0^{\infty}\int_0^{\infty} E(r,\theta,\phi)\\ &\quad\times\exp\{2\pi jRr[\cos\Theta\cos\theta\\ &\quad+\sin\Theta\sin\theta\cos(\phi-\Phi)]\}r^2\\ &\quad\times\sin\theta\,\mathrm{d}R\,\mathrm{d}r\,\mathrm{d}\phi\,\mathrm{d}\theta\end{aligned} \tag{6}$$

To simplify the ODF calculation above, we may first calculate the ODF polar value $\text{ODF}(0,0)$ with $\Theta = 0$ and $\Phi = 0$, i.e.

$$\begin{aligned}\text{ODF}(0,0) = \int_0^{\pi}\int_0^{2\pi} & E(\theta,\phi)\\ &\times\left\{\int_0^1\cos[2\pi jR(\cos\theta)]\sin\theta\,\mathrm{d}R\right\}\mathrm{d}\phi\,\mathrm{d}\theta\end{aligned} \tag{7}$$

where the infinite integration along R coordinate can be normalized to an finite interval $[0,1]$, under consideration of the spherical symmetry of the diffusion anisotropy, i.e. $E(r,\theta,\phi) = E(r,\pi-\theta,\pi+\phi)$. It is noted that the ODF value at arbitrary orientation (Θ,Φ) can be calculated from $\text{ODF}(0,0)$ through a spherical rotation.

2.3. Q-ball imaging

QBI method calculates the ODF of the diffusion process in each voxel by applying a spherical topographic inversion called Funk-Radon transform (FRT) onto the value of unity $|\mathbf{q}|$ acquisition, i.e. the "q-ball". As described in [17], for an arbitrary direction of interest $\mathbf{u}$, an FRT of a spherical distribution $p(\mathbf{u})$ is defined as the integration over the corresponding equator, i.e.

$$\text{FRT}(p(\mathbf{u})) = \int_{w\perp\mathbf{u}} p(\mathbf{w})\mathrm{d}\mathbf{w} \tag{8}$$

where integral vector $\mathbf{w}$ is located in the plane perpendicular to the given direction $\mathbf{u}$. Tuch et al. [18] has demonstrated that the ODF can be well approximated by the FRT of the diffusion signal on the q-ball, such that

$$\text{ODF}(\mathbf{u}) = \text{FRT}(E(\mathbf{u})) = \int_{\mathbf{q}\perp\mathbf{u}} E(\mathbf{q})\mathrm{d}\mathbf{q} \tag{9}$$

Similar to the previous case of DSI method, the calculation of ODF profile can be exemplified by the calculation of the

ODF value at polar angle ($\Theta = 0$, $\Phi = 0$). Thus, we may rewrite Eq. (9) as following:

$$\mathrm{ODF}(0,0) = \int_0^{\pi}\int_0^{2\pi} E(\theta,\phi)W(\theta)\mathrm{d}\phi\,\mathrm{d}\theta \qquad (10)$$

where the weighting function $W(\theta)$ has the unit value only at the place where $\theta = \pi/2$, so as to form the integral path along the equator of the polar direction.

A comparison between Eqs. (7) and (10) indicates that both DSI and QBI methods can resolve the ODF profile through a similar algorithm of integration over the q-ball profile, but using different weighting functions. The integral weighting function used by the DSI method has a "Mexican-hat" shape with a maximum value at $\theta = \pi/2$, corresponding to the equator with respect to the polar axis. For the QBI method, the integral weighting function $W(\theta)$ degenerates to a δ function shape pulse located at the equator position.

2.4. Computer simulations

The diffusion-weighted MR signals and the ADC profiles of a general fiber crossing were generated according to Eqs. (1)–(3). For each intravoxel fiber, the anisotropic parameter was set as $\beta = 0.1$ and the maximal ADC corresponding to the major eigenvalue was set as $\lambda_1 = 1 \times 10^{-3}$ mm^2/s, simulating a white matter tract with fractional anisotropy (FA) value of 0.89. The corresponding ODF profiles were calculated by DSI and QBI methods as described in Eqs. (7) and (10), respectively. Different b values (1000–10,000 s^2/mm) with an interval of 500 s^2/mm were used in the simulations of the diffusion-weighted MR experiments.

Both noise-free and noisy contaminations were simulated in our study. To evaluate the effects of realistic noisy conditions, the Rician-distributed noises were artificially added to the MR signal intensities in the simulated diffusion-weighted experiments. The signal-to-noise ratio (SNR) was set as 20, 40, 60, 80, 100 and 120, respectively, defined for the non-diffusion reference images. According to the analysis in [29], the mean (η) and standard deviation (SD) (σ_η) of the Rician-distributed noise in the magnitude-reconstructed signals can be expressed as $\eta = \sigma\sqrt{\pi/2}$ and $\sigma_\eta = \sqrt{2-(\pi/2)}$, respectively, where σ is the SD of the MR signal.

A total of 181 intersection angles of the fiber crossing were simulated ranging from 0° to 180° with an interval of 1°. For simplicity, the first fiber was placed at a fixed orientation, e.g. the polar direction ($\theta_1 = 0, \phi_1 = 0$), while the second fiber was orientated on a latitude circle according to the intersection angle, i.e. ($\theta_2 = 0 \sim \pi, \phi_2 = 0$). As illustrated in Figs. 1 and 2, each intravoxel fiber produced a pair of centrally symmetric local maxima (at the opposite

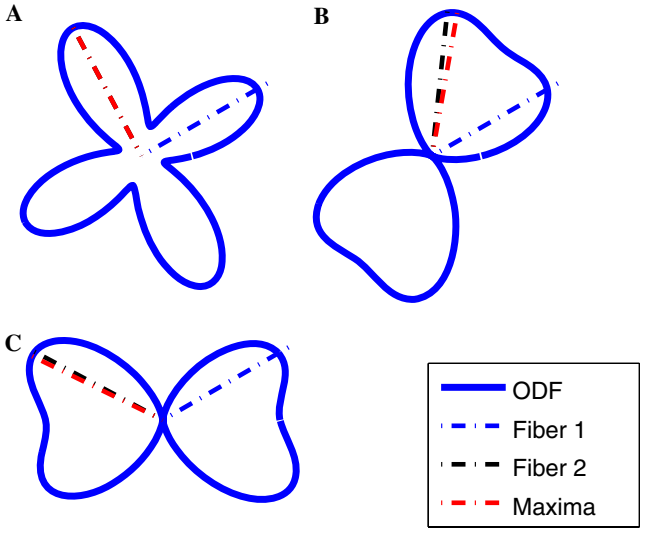

Fig. 1. The two-dimensional ODF profiles (measured by DSI method) of typical slow exchange fiber crossings simulated with $f = 0.5$ and $b =$ of 5000 (s^2/mm). The two intravoxel fibers are placed inside the plane of the paper. The dashed thin lines with blue, black and red colors represent the actual orientation of the fiber 1, fiber 2 and the orientation of fiber 2 estimated by the local maxima on the ODF profile, respectively. (A) The ODF profile of an orthogonal fiber crossing $\Omega_{12} = 90°$. No deviation angle is detected between the profile local maxima and the actual fiber orientation. (B) The ODF profile of a fiber crossing with an acute intersection angle $\Omega_{12} = 56°$. A small deviation angle between the red and black lines represents a slight underestimation of the actual intersection angle. (C) The ODF profile of a fiber crossing with an obtuse intersection angle $\Omega_{12} = 124°$. A small deviation angle between the red and black lines represents a slight overestimation of the obtuse intersection angle. (For interpretation of the references to color in this figure legend, the reader is referred to the web version of this paper.)

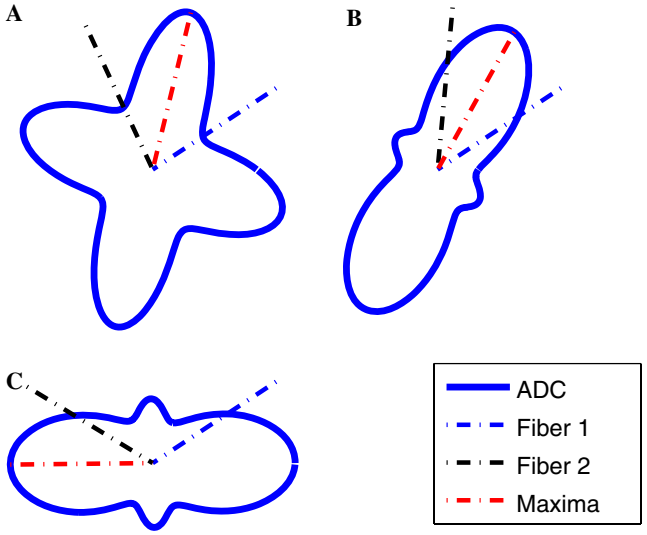

Fig. 2. The two-dimensional ADC profiles of the same fiber crossings as those shown in Fig. 1, simulated with $b = 5000$ (s^2/mm). The dashed thin lines with color of blue, black and red are used to represent the actual orientation of the fiber 1, fiber 2 and the orientation of fiber 2 estimated by ADC local maxima, respectively. (A) The ADC profile of an orthogonal fiber crossing $\Omega_{12} = 90°$. A deviation angle of 45° is spanned between the ADC profile local maxima and the actual fiber orientation. (B) The ADC profile of a fiber crossing with an acute intersection angle $\Omega_{12} = 56°$. A deviation angle of 28° is spanned between the ADC profile local maxima and the actual fiber orientation. (C) The ADC profile of a fiber crossing with an obtuse intersection angle $\Omega_{12} = 124°$. A deviation angle of 28° is spanned between the ADC profile local maxima and the actual fiber orientation. (For interpretation of the references to color in this figure legend, the reader is referred to the web version of this paper.)

directions for each other) on the calculated ODF or ADC profiles. The local maxima produced by the second fiber were identified by an optimization process to achieve the maximum of the ODF or ADC value from an initial point corresponding to the actual second fiber direction (θ_2, ϕ_2). Let (θ_2', ϕ_2') be the spherical coordinates of the estimated local maxima, the estimated fiber intersection angle is defined as $\Omega_{12}' = \Omega[(\theta_2', \phi_2'), (\theta_1, \phi_1)]$, where $\Omega[\bullet, \bullet]$ denotes the angle spanned between 2 directions. Similarly, $\Omega_{12} = \Omega[(\theta_2, \phi_2), (\theta_1, \phi_1)]$ is used to denote the actual intersection angle between (θ_2, ϕ_2) and (θ_1, ϕ_1). The deviation angle of the profile is then given by $\delta\Theta = \Omega_{12}' - \Omega_{12}$. For the ADC profile, the phase-corrected deviation angle can be expressed as

$$\delta\Theta = \begin{cases} \delta\Theta & |D_{CS}^4| < 0.5 \cdot b(\beta+1)\lambda_1 \\ \delta\Theta - \mathrm{ang}\{D_{CS}^4\}/4 & |D_{CS}^4| \geqslant 0.5 \cdot b(\beta+1)\lambda_1 \end{cases} \tag{11}$$

3. Results

3.1. ODF and ADC profiles

A slow-exchange fiber crossing with equal signal contribution was chosen to demonstrate typical behaviors of the ODF and ADC profiles that were estimated with a fixed b value of 5000 s^2/mm. Fig. 1 illustrates the two-dimensional ODF profiles calculated by the DSI method, where subfigures A, B and C correspond to the fiber crossing with intersection angles (Ω_{12}) of 90°, 56° and 124°, respectively. In Fig. 1A, the ODF profile of the orthogonal fiber crossing has a symmetric 4-leaf shape. The local maxima of the ODF profile correspond perfectly to the intravoxel fiber orientations as indicated by the dashed lines, and the estimated fiber 2 (dashed red line) has the same orientation as the actual fiber 2. In Fig. 1B and C, the unevenly distributed ODF maxima result in an angular deviation, i.e. slight underestimation for the acute intersection but over estimation for the obtuse intersection, between the estimated fiber 2 (dashed read line) and the actual fiber 2 (dashed black line).

Similarly, Figs. 2A–C illustrate the two-dimensional ADC profiles of the same fiber crossings with intersection angles of 90°, 56° and 124°, respectively. In Fig. 2A, the intravoxel fibers are actually orientated corresponding to the local *minima* of the ADC profile for the orthogonal fiber crossing. A deviation angle of 45° would be detected if the local maxima method were applied to the ADC profile. In Fig. 2B, the deviation angle between the local maximum and the real fiber orientation is 28°, which is the half of the fiber intersection angle of 56°. In Fig. 2C, the 28° deviation angle lies on the other side from the estimated local maximum to the real fiber orientation. Compared with Fig. 1, the ADC profiles have larger angular deviations (without the phase-correction) than the corresponding ODF profiles.

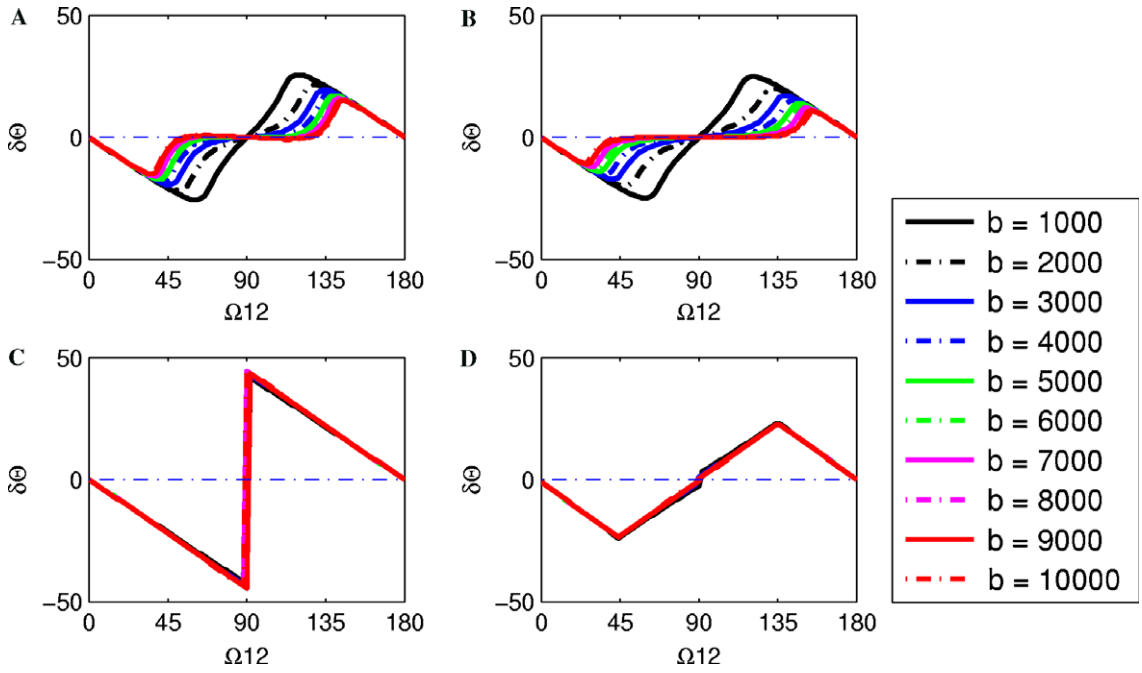

Fig. 3. The effects of b value on the angular deviations with respect to the intersection angle are illustrated in (A–D) for DSI, QBI, ADC before and ADC after phase-correction methods, respectively. In each subfigure, 10 curves correspond to the b values ranging from 1000 to 10,000 (s^2/mm). (A) The angular deviation curves of DSI method. A higher b value leads to smaller deviation magnitudes and a wider angular zone where the angular devotions are negligible. (B) The deviation curves of QBI method have the similar pattern of the DSI curves. Comparatively, QBI curves have slightly smaller deviation magnitudes and wider zones of minimal deviation. (C) The deviation curves of ADC method before phase-correction have a linear relationship with the intersection angle. The 10 curves corresponding to the different b values are overlapped. (D) The deviation curves of ADC method after phase-correction. The angular deviations are significantly reduced compared with (C).

3.2. Effects of b value

The effects of b value on the behavior of the deviation angle were examined using fiber crossings with equal fraction and slow water-exchange. The deviation angles of DSI and QBI methods at various b values are illustrated in Fig. 3A and B, respectively. For the ADC methods, the angular deviations are plotted in Fig. 3C and D for the results before and after the phase-correction, respectively. In each subfigure, 10 deviation angle curves corresponding to b values ranging from 1000 to 10,000 (s^2/mm) are plotted with respect to the fiber crossing intersection angle. All these curves are centrally symmetric about the orthogonal intersection. Negative deviation angles (i.e. underestimation) are observed for the acute intersections, whereas positive angular deviations (i.e. overestimation) occur at the obtuse intersections.

In general, the ODF methods (i.e. DSI and QBI) have very similar behavior, but are different from the ADC methods. The deviation angles of DSI and QBI methods are convergent to zero when the intersection angle approaches to 90°, 0° or 180°. For both DSI and QBI, the magnitudes of the deviation angle reach the peaks of 15°–22° when the intersection angle is around 25°–65°. Under the same b value condition, QBI has a slightly smaller peak deviation magnitude than that of the DSI, and the intersection angle corresponding to the peak deviation is also slightly smaller (for acute intersections) than that of the DSI method. For DSI and QBI methods, the magnitude of the angular deviation is lower when a higher b value is used. The intersection angle corresponding to the peak deviation angle slightly shifts to the lower (for the acute intersections) or higher (for the obtuse intersections) ends with higher b values. It is observed that the shifting of the peak intersection angle tends to be saturated when the b factor approaches very high values (e.g. the 10,000 s^2/mm). For high b values, the angular deviation of DSI and QBI methods are negligible in an zone centered at the 90° intersection. The width of non-deviation zone increases with higher b values, and becomes saturated when the b value is over 10,000 (s^2/mm). Under the same b values, the QBI's deviation angles are slightly (2°–5°) smaller than those of DSI.

As shown in Fig. 3C and D, the angular deviation curves of the ADC methods are almost overlapped for different b values, indicating that the b value has little effect on the angular deviation of the ADC method. Before the phase-correction, the magnitude of deviation angle of the ADC profile is proportional to the intersection angle (the half of the acute intersection angle). When the intersection angle approaches 90°, an abrupt flip of the angular deviations occurs between the two peaks of −45° and 45°. After the phase-correction, the ADC method has maximal deviation of 22.5°, which appears at the 45° and 135° interaction points, whereas the 0° deviation appears at the 90° intersection. In general, angular deviation cures of the ADC method are relatively closer to the ODF methods after the phase-correction. However, the non-deviation zone of the ODF methods cannot be observed around the 90° intersection for the phase-corrected ADC method. For the b values larger than 1000 s/mm^2, the ODF methods generally have smaller angular deviations than the ADC methods, especially for the intersections close to 90°. When the intersection angle approximates 0° or 180°, the angular deviations estimated by the ADC methods are convergent to (or slightly larger than) those of the DSI and QBI methods.

3.3. Effects of imaging noise

Above results were obtained from the noise-free environment. To demonstrate the effects of the Rician-distributed noise contamination in the diffusion-weighted MRI experiments, the angular deviations of the general fiber crossing were estimated by the mean value and the standard deviation (SD). The slow-exchange equal fraction fiber crossing was selected to present the results of the imaging noise effects. The mean and SD of the angular deviations are plotted with respect to the intersection angle in Figs. 4 and 5, under the conditions of b value = 2000 and 5000 (s^2/mm), respectively. In both figures, subfigures A, B, C and D are corresponding to the DSI, QBI, ADC before and ADC after phase-correction methods, respectively. In each subfigure, the solid black curve in the central position represent the mean angular deviations, and the dashed color curves plotted on the upper and lower sides of the mean curve represent the SD ranges of the angular devotions associated with different signal-to-noise ratio (SNR) ranging from 20 to 120, which are defined regarding to the reference images without diffusion weighting. In general, the different noise levels have little effect on the mean angular deviation curves that are completely overlapped, but have significant effects on the SD of the angular deviation.

It is shown that the mean angular deviation curves estimated in the noisy environments show a high consistency with the corresponding noise-free deviation curves, when the same b value is used. Comparing with the noise-free curves illustrated in Fig. 3, the mean angular deviation curves have a sharper transition around the peaks of the mean angular deviation. However, the intersection angles associated with the angular deviation peaks keep the same in the noise-free and noisy environments. For the SD of the angular deviation, it is demonstrated that a higher SNR generally leads to a lower SD value of the angular deviation. The comparison between Figs. 4 and 5 indicates that different b values may have different effects on the angular deviation SD for the ODF and ADC methods. For the intersection angles close to 0° or 180°, the ADC methods generally have a higher SD of the angular deviation, and show a higher sensitivity to the diffusion weighting with a positive correlation between the b value and the

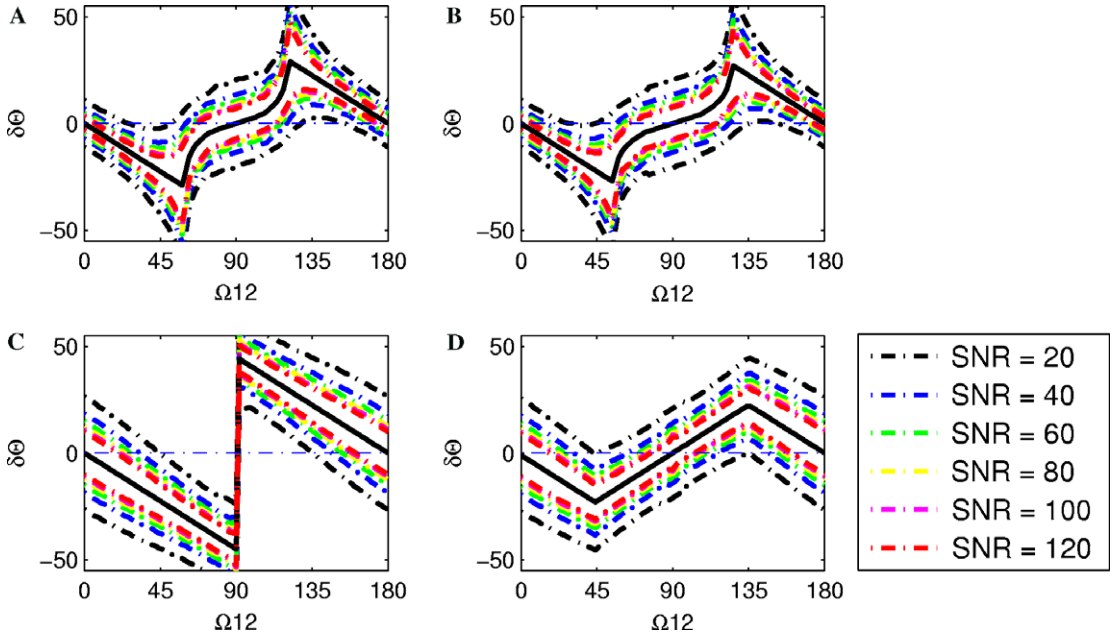

Fig. 4. The effects of the Rician-distributed noise on the angular deviations are illustrated for the slow-exchange fiber crossing under the condition of $b = 2000$ (s^2/mm). (A–D) correspond the DSI, QBI, ADC before and ADC after phase correction methods, respectively. In each subfigure, the solid black curve in the central position represents the mean angular deviations. The dashed color curves on both sides of the mean deviation curve are used to denote the standard deviation range of the angular deviations for SNR from 20 to 120. (A) The noise effects on the angular deviations for DSI method under $b = 2000$ (s^2/mm). (B) The noise effects on the angular deviations for QBI method under $b = 2000$ (s^2/mm). (C) The noise effects on the angular deviations for ADC method before phase-correction under $b = 2000$ (s^2/mm). (D) The noise effects on the angular deviations for ADC method after phase-correction under $b = 2000$ (s^2/mm).

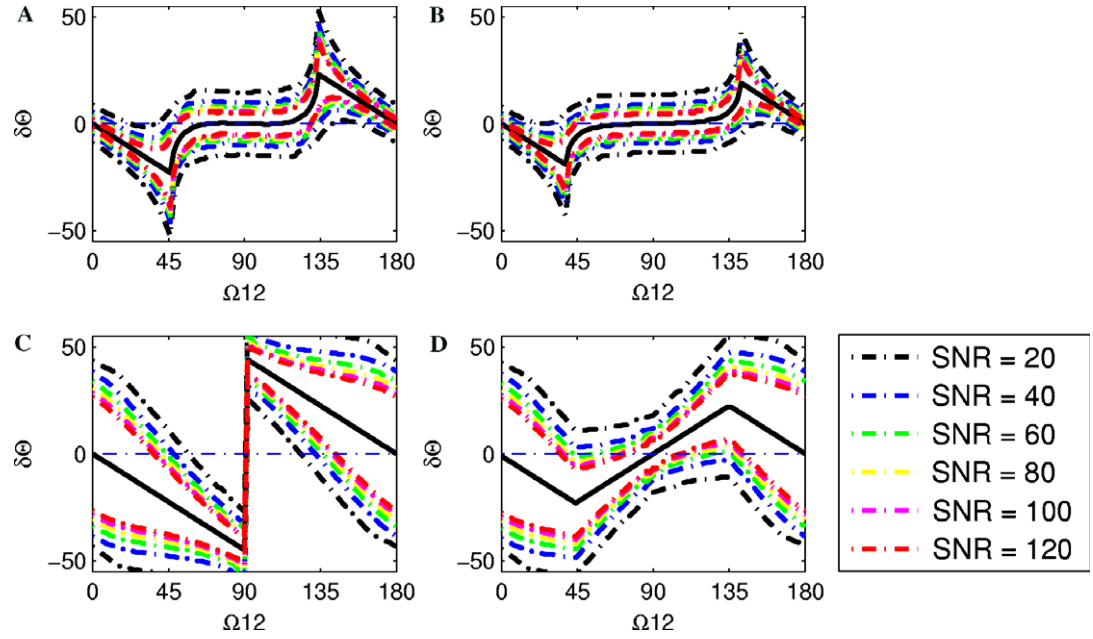

Fig. 5. The effects of the Rician-distributed noise on the angular deviations are illustrated for the slow-exchange fiber crossing under the condition of $b = 5000$ (s^2/mm). (A–D) corresponds the DSI, QBI, ADC before and ADC after phase correction methods, respectively. In each subfigure, the solid black curve in the central position represents the mean angular deviations. The dashed color curves on both sides of the mean deviation curve are used to denote the standard deviation range of the angular deviations for SNR from 20 to 120. (A) The noise effects on the angular deviations for DSI method under $b = 5000$ (s^2/mm). (B) The noise effects on the angular deviations for QBI method under $b = 5000$ (s^2/mm). (C) The noise effects on the angular deviations for ADC method before phase-correction under $b = 5000$ (s^2/mm). (D) The noise effects on the angular deviations for ADC method after phase-correction under $b = 5000$ (s^2/mm).

angular deviation SD. For the DSI and QBI methods, a relatively larger SD of the angular deviations is illustrated around the orthogonal intersection zone where the mean angular deviation approaches zero. It is also indicated that DSI and QBI methods share a similar pattern of the angular deviation SD, and the QBI shows a slightly smaller SD values.

4. Discussion

For the DSI and QBI methods, the angular deviation between the local maxima of the ODF profiles and the actual fiber orientations reflect the imperfection of the q-space methods in delineating intravoxel multiple fibers. For the ADC profiles, the local maxima before the phase-correction do not directly correspond to the fiber orientations. The angular deviations are significantly reduced after the phase correction procedure based on the diffusion circular spectrum method (DCSM). Although previous studies have partially revealed the distortions of the diffusion profiles, the quantification for the angular deviations in this study should be more important, because it could lead to the strategies to improve the non-invasive mapping of neuronal connectivities inside the brain. To focus on the *inherent* angular properties of the diffusion profiles in their original form, the following assumptions have been employed in the simulations: (i) No specific diffusion encoding scheme with limited number of directions was involved in the diffusion weighing simulation. Instead, the local maxima on the profiles were identified by an optimization process with an angular searching step smaller than 0.2°. This technique guarantees that the present simulation results are independent from the number of sampling or the encoding scheme. (ii) No additional post-processing procedures were applied onto the ODF profiles calculated by either DSI or QBI methods, i.e. the ODF profiles used in the present simulations are completely "raw" without any artificial enhancement or distortion. The previous techniques with post-processing for the ODF profiles, as proposed in [17,18,25], are not included in the present investigation.

In the noise-free environment, it has been demonstrated that the systematic angular deviations do exist between the actual fiber orientations and the local maxima of either ODF or ADC profiles estimated by the beyond-tensor diffusion MRI techniques. For all methods, the symmetric pattern of the deviation curves about the 90° intersection is due to the symmetry of the ideal diffusion process, i.e. the ODF (or ADC) value of any diffusion system must have the same intensity on a pair of opposite directions. It is also indicated that both ODF and ADC's local maxima tend to underestimate the acute intersection angles and correspondingly overestimate the obtuse intersection angles. This can be partially explained by the adherence between the two adjacent lobes on the ODF or ADC profile. For a fiber crossing with an acute intersection, for example, the two adjacent lobes on the ODF/ADC profile tend to adhere to each other, resulting in shifts of the pair of local maxima in the direction towards each other. When the intersection angle is particularly small, the deviation curves of all the methods are actually overlapped.

A general fiber crossing can degenerate into a single fiber by approximating the intersection to 0° or 180°. In this case, the simulation results in noise-free environments indicated that the deviation angles of all the methods decrease to zero. On the other hand, when the fiber crossing approximates a "typical" fiber crossing, i.e. a slow-exchange fiber crossing with the orthogonal intersection, the angular deviations behave differently for these methods. In general, the ODF methods (including DSI and QBI) have a relatively wide non-deviation deviation zone centered at the 90° intersection, especially when the b value is larger. This result confirms the ODF methods' ability to accurately estimate the intravoxel fiber orientations for the typical fiber crossings. For the ADC methods, the angular deviations before and after the phase-correction have very different behaviors. Before the correction, ADC profile's angular deviation linearly increases with the intersection angle with a peak magnitude of 45° at the orthogonal intersection, indicating the inability of the original ADC local maxima in inferring the multiple fiber orientations. After the phase-correction, however, the deviations converge to zero for the orthogonal fiber crossing, and the deviation peaks are reduced to 22.5° at the intersections of 45° or 135°.

For the intersections close to 90°, the ODF methods generally show less angular deviations than the ADC method even after the phase correction, especially when the b value is larger than 1000 (s/mm^2). This is because an ADC can be regarded as the measurement of the vector sum of all diffusivities with respect to the measurement direction. Thus, the ADC maximum generally appears in the middle between two crossing fibers. Differently, the ODF value characterizes the probability density of the fiber orientation distribution. A higher consistency between the ODF maxima and the real fiber orientation is generally expectable. It should be noted that the phase DCSM method may not be the only way to do the phase correction for the ADC profiles. Because the DCSM technique can be regarded as a simplified version of spherical harmonic decomposition (SHD) method [22], the phase information of the SHD harmonics may also be utilized to achieve the ADC orientation correction, as discussed in [19].

The b values exert significant effects on the deviation angle behaviors of the ODF methods for the slow-exchange fiber crossings. Use of a higher b value generally results in a reduction of the deviation angle magnitudes and an increase of the non-deviation zone around the 90° intersection. In practice, both DSI and QBI methods acquire data in q-space at relatively large b values as reported in [15–17]. The present results confirm that the ODF methods do have good accuracy in the fiber orientation estimation, especially for those crossings close to 90° intersection. Nevertheless, our simulations also suggest that systematic angular

deviations do exist for the ODF methods, and the peak deviation angle of 18°–25° occurs when the acute intersection angle is around 30°–55°, for the b values ranging from 10,000 to 1000 (s^2/mm), respectively. The QBI method demonstrates a slight yet consistent advantage over the DSI method with smaller deviation angles under the same conditions of intersection angle, signal fraction and b value. Unlike the ODF methods, the b values have little effects on the angular deviations of the ADC profiles, although the *shape* of the ADC profiles have been significantly changed by the b values as reported in [19,20].

In the noisy environments, the estimated mean angular deviations show a good consistency with the angular deviations measured in the noise-free environment. This property justifies that the present noise-free angular deviation results are still useful in estimating the actual angular deviation in noisy conditions, provided that this estimation can be repeated for many times until a stable average of the deviation angles is reached. As revealed in [30], the non-Gaussian property of the noise would result in the systematic distortion of the diffusion profiles. The present study, however, suggests a positive perspective because the noise would not result in significant bias of the mean angular deviation. Our simulations also indicate that the estimated angular deviation angles of a typical orthogonal fiber crossing would be distributed in a standard deviation range of 7°–20°, corresponding to the SNR from 120 to 20 in the diffusion reference image. Compared with the ADC method, the ODF methods show stronger robustness against the noise contamination for the intersection angles close to 0° or 180°, especially in high b value conditions. In terms of standard deviation of the angular deviations, a slight superior of the noise robustness can be also observed for the QBI method over the DSI method.

5. Conclusion

The present study has systematically investigated the angular deviations between the local maxima on different diffusion profiles and the actual fiber crossing orientations for DSI, QBI and ADC methods. A slow-exchange fiber crossing with varying intersection angles and signal fractions was used to generate the ODF and ADC profiles and to assess angular deviations. In general, all the methods are apt to underestimate acute intersection angles and overestimate obtuse intersection angles. For a typical fiber crossing, the angular deviation of ODF methods is minimal around the 90° intersection. Originally, the ADC method has a deviation angle proportional to the intersection angle, with a peak at the orthogonal intersection. After the phase-correction, the angular deviations are significantly reduced. The QBI method demonstrates a slight, yet consistent, advantage of less deviation over the DSI method under the same conditions. Higher b values are favorable for achieving lower angular deviations in both DSI and QBI methods, but have little effect on the ADC method. In the noisy environments, the mean angular deviations show a good consistency to the angular deviation estimated in corresponding noise-free environment.

Acknowledgment

This research was supported by the Intramural Research Program of the NIH, the National Institute on Drug Abuse.

References

[1] P.J. Basser, J. Mattiello, D. Le Bihan, Estimation of the effective self-diffusion tensor from the NMR spin echo, J. Magn. Reson. 103 (1994) 247–254.
[2] P.J. Basser, C. Pierpaoli, Microstructural and physiological features of tissues elucidated by quantitative-diffusion-tensor MRI, J. Magn. Reson. Series B. 111 (1996) 209–219.
[3] D. Le Bihan, J.F. Mangin, C. Poupon, C.A. Clark, S. Pappata, N. Molko, H. Chabriat, Diffusion tensor imaging: concepts and applications, J. Magn. Reson. Imag. 13 (2001) 534–546.
[4] R. Xue, P.C.M. Van Zijl, B.J. Crain, M. Solaiyappan, S. Mori, In vivo three-dimensional reconstruction of rat brain axonal projections by diffusion tensor imaging, Magn. Reson. Med. 42 (1999) 1123–1127.
[5] T.E. Conturo, N.F. Lori, T.S. Cull, E. Akbudak, A.Z. Snyder, J.S. Shimony, R.C. McKinstry, H. Burton, M.E. Raichle, Tracking neuronal fiber pathways in the living human brain, Proc. Natl. Acad. Sci. USA 96 (1999) 10422–10427.
[6] P.J. Basser, S. Pajevic, C. Pierpaoli, J. Duda, A. Aldroubi, In vivo fiber tractography using DT-MRI data, Magn. Reson. Med. 44 (2000) 625–632.
[7] C. Poupon, J.F. Mangin, C.A. Clark, V. Frouin, J. Régis, D. Le Bihan, I. Bloch, Towards in inference of human brain connectivity from MR diffusion tensor data, Med. Imag. Anal. 5 (2001) 1–15.
[8] A.L. Alexander, K.M. Hansan, M. Lazar, J.S. Tsuruda, D.L. Parker, Analysis of partial volume effects in diffusion-tensor MRI, Magn. Reson. Med. 45 (2001) 770–780.
[9] P.J. Basser, Relationship between diffusion tensor and q-space MRI, Magn. Reson. Med. 47 (2002) 392–397.
[10] Y. Assaf, Y. Cohen, Assignment of the water slow-diffusing component in the central nervous system using q-space diffusion MRS: implications for fiber tract imaging, Magn. Reson. Med. 43 (2000) 191–199.
[11] M.D. King, J. Houseman, D.G. Gadian, A. Connelly, Localized q-space imaging of the brain, Magn. Reson. Med. 38 (1997) 930–937.
[12] P.T. Callaghan, PGSE-MASSEY, a sequence for overcoming phase instability in very high-gradient spin-echo NMR, J. Magn. Reson. 88 (1990) 493–500.
[13] Y. Assaf, R.Z. Freidlin, G.K. Rohde, P.J. Basser, New modeling and experimental framework to characterize hindered and restricted water diffusion in brain white matter, Magn. Reson. Med. 52 (2004) 965–978.
[14] V.J. Wedeen, T.G. Reese, D.S. Tuch, M.R. Wiegel, R.M. Dou, R.M. Weiskoff, D. Chessler, Mapping fiber orientation spectra in cerebral whiter matter with Fourier-transform diffusion MRI, in: Proceedings of the 8th Annual Meeting of ISMRM, Denver, 2000, pp. 82.
[15] C.P. Lin, V.J. Wedeen, J.H. Chen, C. Yao, W.Y. Tseng, Validation of diffusion spectrum magnetic resonance imaging with manganese-enhanced rat optic tracts and *ex vivo* phantoms, NeuroImage 19 (2003) 482–495.
[16] D.S. Tuch, T.G. Reese, M.R. Wiegell, V.J. Wedeen, Diffusion MRI of complex neural architecture, Neuron 40 (2003) 885–895.
[17] D.S. Tuch, Q-ball imaging, Magn. Reson. Med. 52 (2004) 1358–1372.
[18] D.S. Tuch, R.M. Weisskoff, J.W. Belliveau, V.J. Wedeen, High angular resolution diffusion imaging of the human brain, in: Proceedings of the 7th Annual Meeting of ISMRM, Philadelphia, 1999, pp. 321.

[19] L.R. Frank, Anisotropy in high angular resolution diffusion-weighted MRI, Magn. Reson. Med. 45 (2001) 935–939.
[20] D.C. Alexander, G.J. Barker, S.R. Arridge, Detection and modeling of non-Gaussian apparent diffusion coefficient profiles in human brain data, Magn. Reson. Med. 48 (2002) 331–340.
[21] L.R. Frank, Characterization of anisotropy in high angular resolution diffusion weighted MRI, Magn. Reson. Med. 47 (2002) 1083–1099.
[22] W. Zhan, H. Gu, S. Xu, D.A. Silbersweig, E. Stern, Y. Yang, Circular spectrum mapping for intravoxel fiber structures based on high angular resolution apparent diffusion coefficients, Magn. Reson. Med. 49 (2003) 1077–1088.
[23] W. Zhan, E.A. Stein, Y. Yang, Mapping the orientation of intravoxel crossing fibers based on the phase information of diffusion circular spectrum, NeuroImage 23 (2004) 1358–1369.
[24] E.A.H. von dem Hagen, R.M. Henkelman, Orientational diffusion reflects fiber structure within a voxel, Magn. Reson. Med. 48 (2002) 454–459.
[25] E. Ozarslan, T.M. Spepherd, B.C. Vemuri, S.J. Blankband, T.H. Mareci, Resolution of complex tissue microarchitecture using the diffusion orientation transform (DOT), NeuroImage 31 (2006) 1086–1103.
[26] E.W. Hsu, S. Mori, Analytical expressions for the NMR apparent diffusion coefficients in an anisotropic system and a simplified method for determining fiber orientation, Magn. Reson. Med. 34 (1995) 194–200.
[27] A.L. Alexander, K.M. Hansan, G. Kindlmann, D.L. Parker, J.S. Tsuruda, A Geometric analysis of diffusion tensor measurements of the human brain, Magn. Reson. Med. 44 (2000) 283–291.
[28] D. Le Bihan, E. Breton, D. Lallemand, P. Grenier, E. Cabanis, M. Laval-Jeantet, MR imaging of intravoxel incoherent motions: application to diffusion and perfusion in neurologic disorders, Radiology 161 (1986) 401–407.
[29] H. Gudbjartsson, S. Patz, The Rician distribution of noisy MRI data, Magn. Reson. Med. 34 (1995) 910–914.
[30] D. Jones, P.J. Basser, Squashing peanuts and smashing pumpkins: How noise distorts diffusion-weighted MR data, Magn. Reson. Med. 52 (2004) 979–993.